



Energy absorbing 4D printed meta-sandwich structures: load cycles and shape recovery

Annamaria Gisario¹ · Maria Pia Desole¹ · Mehrshad Mehrpouya² · Massimiliano Barletta³

Received: 12 April 2023 / Accepted: 22 May 2023 / Published online: 1 June 2023
© The Author(s) 2023

Abstract

The present study investigates the behavior of solid cellular structures in polylactic acid (PLA) achieved by FDM technology (fusion deposition modelling). The geometries are permanently deformed by compressive stress and then subjected to shape recovery through the application of a thermal stimulus. The structures are submitted to medium–high and medium–low compression stresses, evaluating the mechanical properties and the absorption energy as the number of cycles varies. The study shows that the ability to absorb energy is related to the density of the model, as well as the degree of damage observed, which increases with increasing number of load cycles. The strongest geometry is the lozenge grid, which is the most reliable. It shows no damage with increasing compression cycles and keeps its capability to absorb energy almost constant. The increase in lozenge grid density leads to an improvement in both mechanical strength and absorption energy, as well as a lower incidence of microcracks in the geometry itself due to the repeated load cycles. These results open up a broad spectrum of applications of custom-designed solid cellular structures in the field of energy absorption and damping.

Keywords 4D printing · Metamaterials · Energy absorbing · Springback · Shape recovery

1 Introduction

Metamaterials are innovative materials artificially engineered to exhibit mechanical, thermal, acoustic, or electromagnetic behavior not found in other naturally occurring materials [1, 2, 3, 4]. Their applications can be multiple and declinable in different sectors, from civil to biomedical, from electronics to aerospace, and in the broader manufacturing sector [5, 6, 7].

Their development goes well with the growing interest in additive manufacturing technologies, which are very competitive with respect to traditional manufacturing

technologies due to the greater possibilities they offer in obtaining intricate shapes, of good quality and in reasonable times [8, 9, 10, 11, 12]. By exploiting additive manufacturing technology, it is in fact much easier to create products with complex architectures. It is possible to set up articulated addition paths of the material that generate reticular structures, with modular cavities and at the same time with mechanical properties comparable to those of a solid artefact [13]. In the conception of new reticular geometries, the study of printing supports constitutes a delicate phase of the process. An attempt is made to drastically limit their use as the presence of supports determines an increase in the cost-per-part due to the time required for their removal and surface finishing operations. It is therefore convenient to produce lattice structures making sure that the lattices themselves act as internal supports and are at the same time capable of withstanding external stresses.

In recent years, the targeted design of metamaterials with lattice structures has garnered significant interest from the scientific community and has involved the use of a wide range of materials, both metallic [14, 15] and polymeric [11, 16]. The unique properties that can be obtained from lattice structures when examined from a mechanical point of view are high stiffness and mechanical strength

✉ Massimiliano Barletta
massimiliano.barletta@uniroma3.it

¹ Dipartimento Di Ingegneria Meccanica E Aerospaziale, Sapienza Università Di Roma, Via Eudossiana 18, 00184 Rome, Italy

² Department of Design, Production, and Management (DPM), University of Twente, Drienerloaan 5, 7522 NB Enschede, The Netherlands

³ Dipartimento Di Ingegneria Industriale Elettronica E Meccanica, Università Degli Studi Roma Tre, Via Della Vasca Navale 79, 00146 Rome, Italy

or greater energy absorption in relation to reduced weight and lower density [17, 18, 19, 20]. The mechanical attributes of AM fabricated parts with lattice structures have been investigated by many researchers following various approaches. In terms of geometries, attention has been paid to structures with triangular, square, circular, or hexagonal lattices. Geometries with auxetic behavior have also been studied, with chiral and non-chiral or bio-inspired forms [1, 2, 3, 4, 5, 6, 7, 8, 9, 10, 11, 12, 13, 14, 15, 16, 17, 18, 19, 20, 21, 22, 23, 24, 25, 26, 27, 28, 29, 30]. Lubombo and Huneault [31], for example, investigated the stiffness and strength under uniaxial tensile and bending loading of PLA thermoplastic cellular structures fabricated by fused filament fabrication (FFF). In particular, five different filling models are examined for which a different mechanical response is highlighted. The hexagonal structure showed good performance with a twofold increase for stiffness and up to 82% for resistance under load. Honeycombs are among the most used to evaluate the performance of cellular materials, perhaps also due to their wide commercial use. In McGregor et al. [32] an in-depth study of the hexagonal lattice that is fabricated by AM using three different thermoplastic polymers is reported: (rigid polyurethane (RPU, $E = 1900$ MPa), additive epoxy (EPX, $E = 3140$ MPa), and cyanate ester (CE, $E = 4200$ MPa)). The mechanical behavior under compressive load of the different materials is evaluated. By varying the relative density in a sufficiently wide range (from 0.06 to 0.23), the results obtained demonstrated the possibility of varying the specific modulus and the specific strength by more than two orders of magnitude. However, a correlation was not made between geometry and the capacity of the structure to absorb energy. Also, Santos et al. [33] have studied honeycomb and auxetic structures (with negative Poisson's ratio) by comparing the behavior of PLA (polylactic acid) and PETG (transparent polyethylene terephthalate modified with glycol). In this case, the ability of the structures to absorb energy as a function of the material and the initial load of the test is investigated. However, a limited number of geometries are analyzed in the work. It should be noted that both polymers examined in this study can be included in the category of shape memory polymers (SMPs), i.e., those intelligent polymeric materials that have the ability to return from a deformed state (temporary shape) to their original shape (permanent) following an external stimulus (trigger), such as for example a change in temperature. SMPs can in fact be profitably employed in the 3D fabrication of metamaterials with reticular structures with the aim of referring to a printing process that will not only be 3D, but 4D, as it takes into account a fourth variable, i.e. time [34].

Stress-induced permanent deformation would imply a one-time use for a traditional polymer. A shape memory

material such as PLA could, on the other hand, allow a repeated use of the manufactured part, through the application of simple external stimuli. The fabrication of a lattice-structured metamaterial can then be promoted for the purpose of lightening the part and to ensure good strain energy absorption capacity but also to ensure the reusability of the fabricated part. Over time, it is therefore possible, by restoring the initial shape, to foresee the use of the part manufactured in PLA over a number of cycles which obviously depends on the specific shape of the lattice as well as on the properties of the material involved. PLA is also a biodegradable polymer with low environmental impact [35] which can easily be processed through additive manufacturing technologies and offer good mechanical performance [36].

In Barletta et al. [37], a study was addressed on the shape recovery capacity of AM reticular structures in PLA following compressive deformations. The parameters of the FDM printing process were varied: nozzle temperature, deposition speed, layer thickness, and then the activation temperature in the thermal stimulus phase was varied. Experimental evidence has highlighted the latter as the most significant parameter for triggering the recovery of the initial shape in the shortest possible time.

Mehrpouya et al. [38] performed a study on the functional behavior of AM lattice structures fabricated by two different SMPs: PLA and C8. In particular, the impact of design and process parameters on maximum compressive load and energy absorption capacity were analyzed. The research shows that on two structural configurations analyzed, one origami-based and the other auxetic-based anti-chiral, the energy absorption is more marked for the former thanks to its better deformation capacity. Furthermore, with the same structure, C8 can withstand lower forces and deformations than PLA. The nozzle temperature, the height of the printed layer, and the printing speed, if properly set, can increase the mechanical strength and energy absorption values of the samples for both materials.

With reference to energy absorption, Yousefi et al. [39] proposed a high-performance auxetic metastructure with an original design inspired by a snowflake. Two materials with distinct mechanical characteristics were tested: the soft hyper-elastic TPU, capable of withstanding large deformations, and the hard elasto-plastic PA12, more performing in terms of energy absorption. The recovery of shape under cyclic loads was analyzed, although in this case, the recovery should be considered spontaneous and not imparted through stimulus. The responses of the two materials are compared in terms of absorbed energy, dissipated energy, and specific energy absorption (SEA) which represents the dissipated energy per unit mass.

To date, however, studies have focused on the evaluation of plastic deformations and performance in terms of energy absorption exhibited by lattice structures as a function of the

materials [20] and the geometries themselves, without however adequately addressing the role of loading and recovery cycles. Furthermore, the current scientific panorama lacks an analysis capable of relating the geometry of the structure with the recovery properties of the initial shape, as well as an analysis of the energy absorption capacity as the state of damage varies as the number of load cycles increases. These considerations could be extended to structures with a cellular pattern even when subjected to dynamic and not only static tests [40, 41].

The aim of this work is, therefore, to study the performance offered by cellular reticular structures when subjected to a suitable compressive stress and to evaluate their ability to absorb energy. Exploiting the shape recovery property of the material, we then want to analyze how the subsequent shape recovery (through thermal stimulation) can make it possible to reiterate the application of the stress over several cycles. For this purpose, various chiral cellular lattice structures have been considered, some of which are already known in the literature and others created ex-novo. The structures were fabricated using FDM (fusion deposition modeling) technology as it represents the most congenial and low-cost additive manufacturing process for PLA. A special procedure has been set up to operate a comparison between the various structures when they are subjected to quasi-static compressive deformation. An attempt was made to identify the correlations between mechanical properties and lattice structure, investigating the aspects that govern the response of SMPs, also in terms of energy absorbed following residual deformation. At the end of the experimental investigation, the structure corresponding to the best response in terms of absorbed energy and recovered deformation per number of cycles was identified. Finally, its density has been increased, therefore the number of cells, in order to understand how this parameter can condition the process of deformation and recovery of the same.

2 Materials and methodologies

The material used for the experimentation is a non-technical PLA filament from Ultimaker (Ultimaker, Utrecht, Netherlands). It is an easily printable material and suitable for producing pieces with good surface quality and mechanical resistance [42]. The diameter of the filament is 2.85 ± 0.10 mm, and the density is 1.24 g/cm^3 . The coloring is green, and this is specified because the mechanical properties can be influenced by the additives necessary to guarantee the coloring [43, 44].

2.1 Definition of the geometries

In the present work, six geometries have been considered, paying particular attention to the chiral structures

characterized for the most part by the presence of connections through arms and circles. In the selected structures, the union between the elements is not to be considered the same for all. To each circular element, it is possible to connect 4 or 6 elements. In the first case, the adjacent circles are located along 4 directions at 90° , while in the second case along 6 directions at 60° to each other. The only geometry, also chiral, which has no connection between arms and circles is the so-called lozenge grid, composed of open lozenge elements. This structure has already been analyzed in a previous study [37] and therefore chosen to have a comparison between a structure that has right angles and one that has circumferences and arms. With the development of these patterns, 3D models consisting of cubes with a side of 30 mm were then created in the CAD environment, using the “Autodesk Inventor 2021” software. Each of the upper and lower faces is delimited by a layer, respectively defined as the top and bottom layer, with dimensions of 32×32 mm. The size of the layers increased by 1 mm per side helps to favor a more gradual distribution of stresses and an increase in the adhesion surface with the plates used during the compression test, as well as the clamping of the specimens during the subsequent shape recovery tests. Table 1 shows the names of the selected structures with the corresponding adjacencies. The values of the relative density ρ^* calculated by SW are also reported. Figure 1 shows the CAD models of the geometry subjected to analysis.

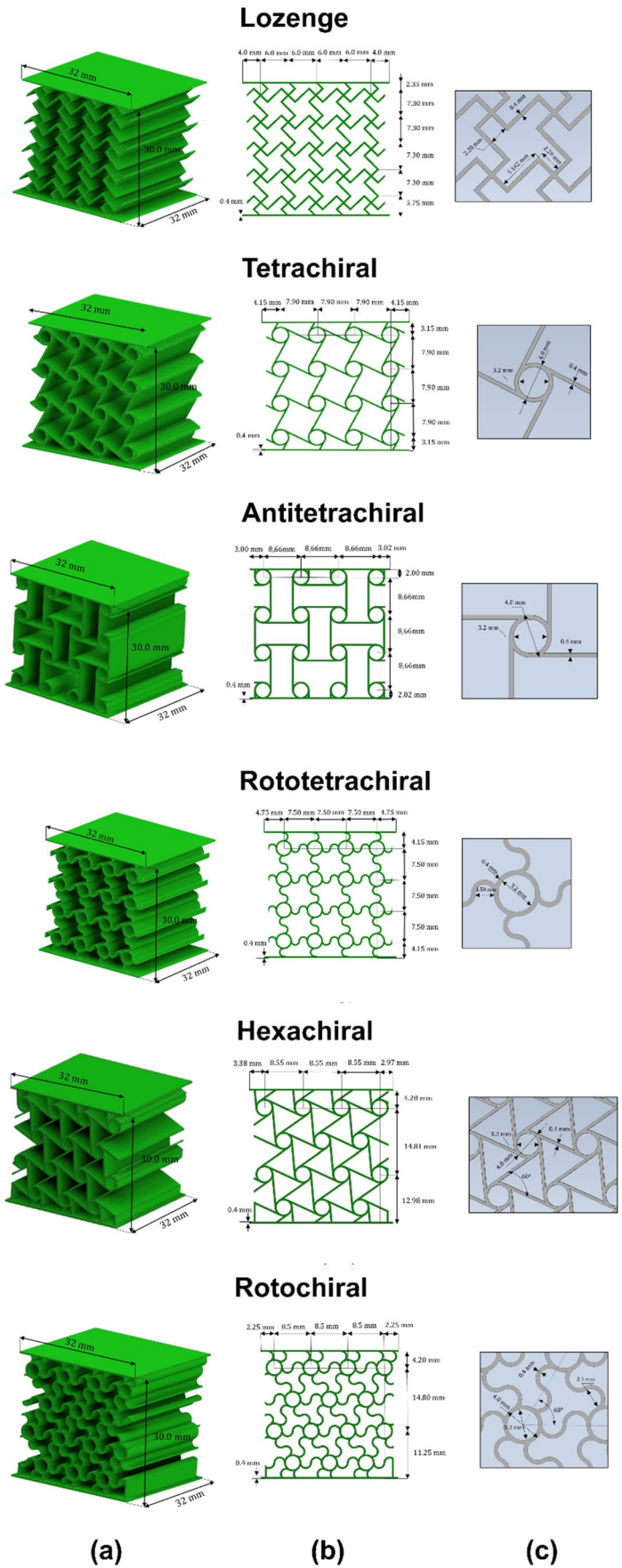
2.2 3D printing process

“Ultimaker S5” (Ultimaker, Utrecht, Netherlands) 3D printer was used, which uses FDM technology. The CAD models have been converted to *.stl, using the “Ultimaker Cura” software (version 4.13.1). The typical printing parameters were set; the layer thickness, the printing temperature, and the printing speed were adjusted, respectively, set at 0.2 mm, 200°C , and 50 mm/s. For the density of the filling elements of the structure, it was set a value of 100%, so as not to have problems in terms of mechanical resistance. It was preferred to position the specimens in the center of the dish so that good thermal uniformity was better guaranteed. Between the printing plate and the lower face of the pattern, a layer

Table 1 Relative density for each geometry

Geometry	Density
Chiral grid (with circular elements)	ρ^*
No. of adjacencies	
4	Antitetrachiral
	Tetrachiral
	Rototetrachiral
6	Hexachiral
	Rotochiral
Lozenge grid	0.154

Fig. 1 3D CAD model: **a** 3D model; **b** front view; **c** cell size



manufactured using PVA (polyvinyl alcohol), a water-soluble polymer, with a thickness of 1 mm has been interposed which forms a support to be removed later but which allows not to create unevenness between the side walls. In fact, a temperature of 50 °C of the printing plate would favor greater crushing of the layer of polymer deposited therein.

2.3 Compression tests

The specimens were subjected to the uniaxial compression test along the direction perpendicular to the top and bottom layer. The tests were performed at room temperature using the “Autograph AGS-X series” universal testing machine (Shimadzu, Kyoto, Japan), equipped with a 5-kN load cell, which guarantees an accuracy of 0.5%. The standard used for carrying out the test is ASTM C365, suitable for compression testing of sandwich structures made of polymeric material.

The compression tests were carried out in successive steps. As a preliminary step, a group of specimens was subjected to a limit displacement of 15 mm and corresponding to half the height of the specimens. Subsequently, once the structures showing the most distinctive behaviors had been identified, a second group of specimens was analyzed and subjected to a lower displacement of 8 mm, such as not to cause irreversible damage to the structure as the load cycles increased. In both cases, the plate lowering speed was 3 mm/min. For each group, three replicas were tested for each pattern in order to verify that the mechanical behavior exhibited by the various structures was sufficiently stable. Replications were especially necessary because chiral structures characterized by the presence of circular elements have a high number of jointing elements between the circles and can be more prone to manufacturing defects during the printing process.

2.4 Springback

Immediately before and after the compression test, the height of the specimens was measured using a vernier caliper. The project dimensions in the CAD model have been fixed, as mentioned, equal to $30 \times 30 \times 30 \text{ mm}^3$. However, once the specimens were made using FDM technology, it was found that the real dimensions were different from the design ones. This is attributable to small shrinkage phenomena of the extrudate during the deposition phase which generates small deviations from the expected measurement [45]. The Table 2 shows, for both groups, the average values of the measurements carried out on the specimens after the manufacturing process and therefore before the compression test.

The measurements taken immediately after the compression test were performed in several intervals. Following preliminary measurements, it was found that after 1 h,

Table 2 Starting values of the heights of the specimens

	Group I/Group II
Tetrachiral	30.10
Antitetrachiral	30.31
Lozenge grid	30.15
Rototetrachiral	30.98
Hexachiral	30.10
Rotochiral	30.25

the structures maintain their height unchanged. For these reasons, the springback phenomenon was analyzed, in both tests at 15 mm and at 8 mm, by measuring the heights of the specimens for 1 h, at time intervals of 5 min. From the comparison between the first set of measurements and the second, it is possible to derive the immediate amount of springback.

2.5 Shape recovery

Subsequently, the shape recovery tests were carried out, i.e., immediately after the measurements of the springback. In order to trigger the shape recovery process, the material must be given an adequate thermal stimulus. The deformed samples were then heated above the glass transition temperature T_g (which is about 60 °C for PLA). This was done by immersing the samples in a temperature-controlled water bath set at 75 °C. For this purpose, a “Corio series C” immersion thermostat (Julabo GmbH, Seelbach, Germany) was used, lowered inside a transparent tank with a capacity of 19 L. Shape recovery analysis was performed via software. In this regard, the tank was filled with 70% distilled water and 30% natural water, in order to prevent the excessive accumulation of residue from changing the chemical-physical properties of the bath over time, making it less reliable the acquired images. Furthermore, an immersion system was designed consisting of a base with a special clamp for housing the sample and a handlebar, which made it possible to reduce the transitory phase of the immersion to a minimum. Recordings were made with a full HD camcorder (GZ-E205, JVC, Yokohama, Kanagawa, Japan). As far as the tracker is concerned, an evolution frequency of 0% has been set to avoid any type of drift from the selected model. This ensures that the point chosen by the system is always selected from the same set of points, defined by the color profile. To minimize the effect of image deformation due to both optics and water refraction, the markers placed to the left of the top layer were mainly used, which are also the closest to the ruler useful for calibrating the analyses. Figure 2 shows a frame taken from the video used to evaluate the

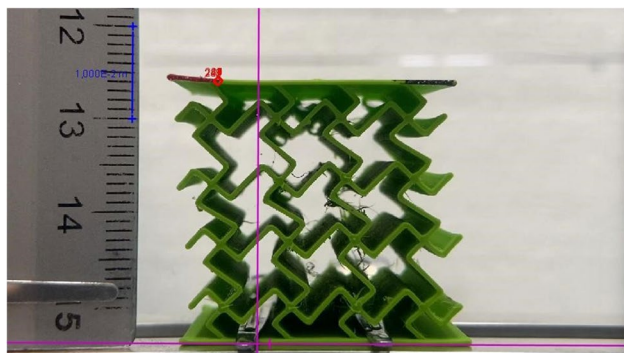


Fig. 2 Tracking software screen

shape return of the lozenge structure in which it is possible to observe the two markers referred to.

2.6 Analysis of the deformation cycles and subsequent recovery of the shape

The developed procedure is characterized by the phases of compression, measurement of the springback, and evaluation of the return of shape. The above procedure was carried out over two cycles for the group of structures subjected to a compression of 15 mm (medium–high stress), while it was repeated over 8 cycles for the second group of structures subjected to a compression of 8 mm (stress medium–low). It was not considered appropriate to continue further as in both cases the structures were permanently damaged at the end of the last loading cycle. It is considered useful to point out that in the case of medium–low compressive stress, the compression and recovery tests could not be conducted continuously, but it was necessary to divide the cycles into three groups of analyses: I and II cycles; III, IV, and V cycles; VI, VII, and VIII cycles. The analysis groups were conducted 48 h apart.

3 Results and discussion

3.1 Analysis of the behavior of structures subjected to medium–high compressive stress

3.1.1 Compression test at 15 mm

Figure 3 shows the force–displacement diagrams of the compression tests for the 6 planned structures. It can be highlighted how the hexachiral and rotochiral structures are able to reach higher resistance. This is in line with what was stated by Gibson et al. (1997) which relates the resistance to the relative density. The cellular structures characterized

by a greater ratio between the areas, therefore with a higher relative density, are also the more resistant ones. The compression curves, however, make it possible to distinguish two phases which correspond to different mechanical behaviors based on the amount of displacement imposed. When the latter does not exceed values between 8 and 10 mm, a rapid increase in force is observed in the initial phase and, depending on the geometries analyzed, the value reached can be in the range 250 N ÷ 1000 N. The lowest value is recorded for the lozenge structures while the highest values for the hexachiral and rotochiral structures. This value is reached in all cases within the first 2 mm and is almost constant for the following 6 ÷ 8 mm. In reality, for each structure, the presence of three peaks is identified which is indicative of the deformation in the longitudinal direction and which sees the consecutive activation of the cells placed in each of the three layers. The descending phase of the peak corresponds to the yielding and consequent deformation of the arms that build the row of cells. The reduction in resistance is caused by the deformation and the consequent variation in the directions of application of the force.

In the case of the lozenge structure, there are no peaks in the compression curves, and it is the only one that does not have circular elements. Therefore, it can be hypothesized that structures that include circular elements have a greater tendency to collapse, but with the same density they are able to support a greater load [46], in some cases even double. This aspect also seems to confirm the study by Orhan and Erden [47], where the lozenge appears to be the least resistant of the structures analyzed.

For displacements greater than 10 mm, the force exerted by the specimens increases significantly, especially for geometries with higher densities. In particular, the structures which have circumferential elements undergo a high deformation, with the contact of all the elements present inside the structure, such as to stiffen the structures with respect to the initial condition. Furthermore, from the analysis of the graphs, it is evident that the variation in behavior between the different structures is very accentuated, due to a certain variability in the way in which the structure is packed. The antitetrachiral and hexachiral structures respond to the compressive stress both with a deformation of the arms and with a rotation of the circumferences. The density of the structures affects not only their mechanical resistance but also the way in which the deformation evolves, as already found in Tancogne-Dejean et al. [48]. Figure 4 shows a frame of the 15-mm compression test for the six structures. The structures characterized by a higher density are subjected, during the compression test, to a packing of the cells inside the structure and in axis with the direction of compression. This is in fact true for the hexachiral, the antitetrachiral, and the rotochiral structures which correspond to the higher densities.

Fig. 3 Force–displacement curves for the preliminary compression tests at 15 mm with mean and standard deviation

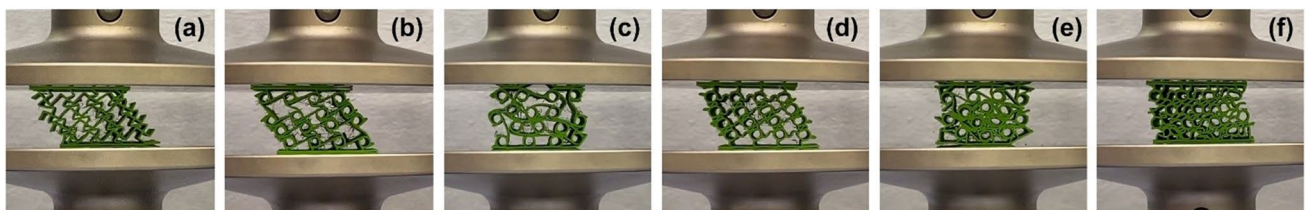
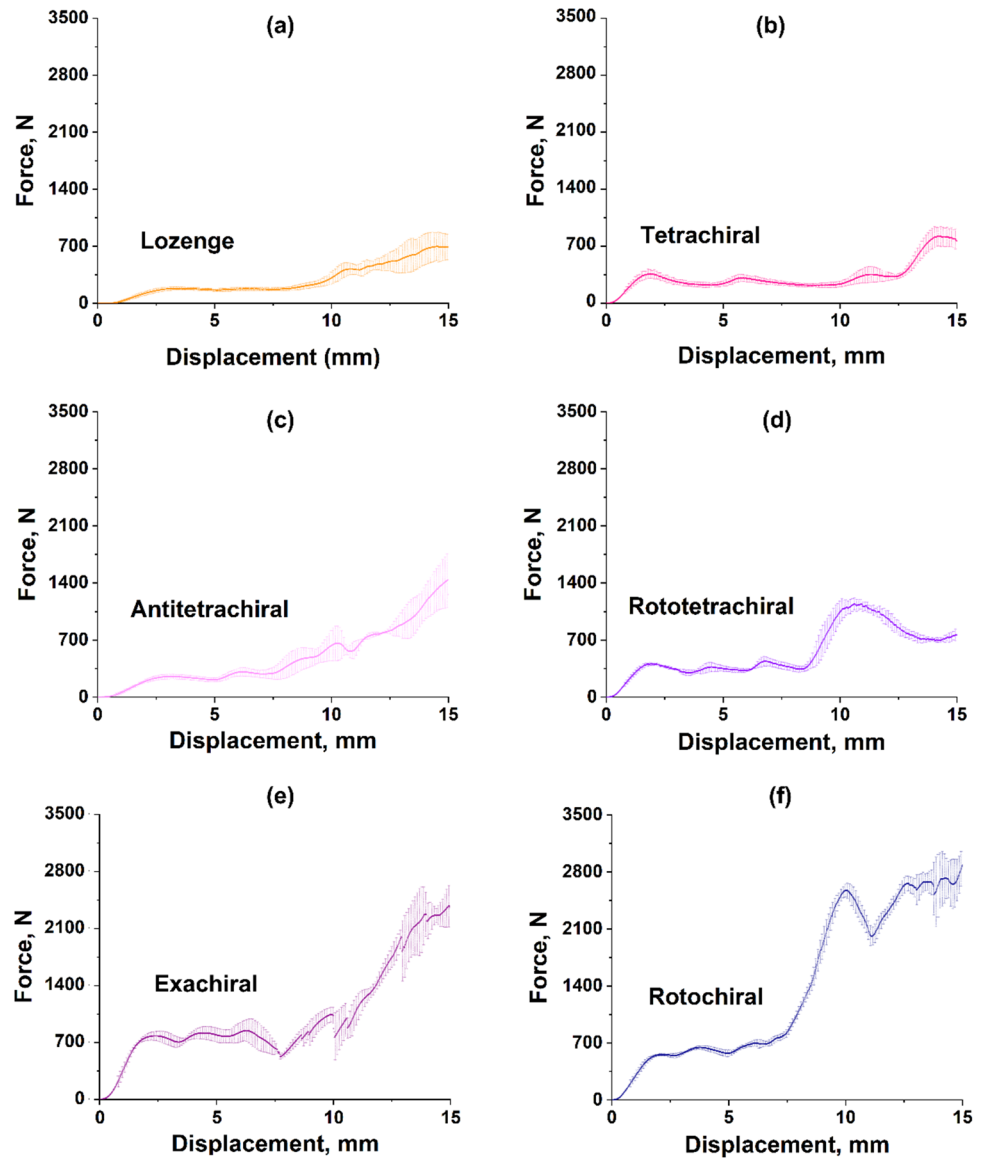


Fig. 4 (a) Lozenge grid; (b) Tetrachiral; (c) Antitetrachiral; (d) Rototetrachiral; (e) Hexachiral; (f) Rotochiral

3.1.2 Springback

At the end of the compression test, the springback was measured on each of the three replicas. In particular, the difference in height detected between the time t_0 , coinciding

with the end of the last compression phase which sees the sample still included between the two plates, and the time t_1 corresponding to 60 min elapsed from the detachment of the dishes was considered. Figure 5 shows the trend of the measurements which highlights how the lozenge structure is

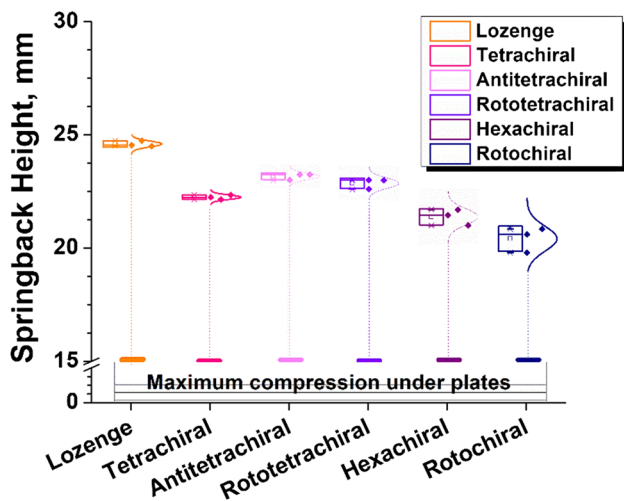


Fig. 5 Box plot springback trials at 15 mm

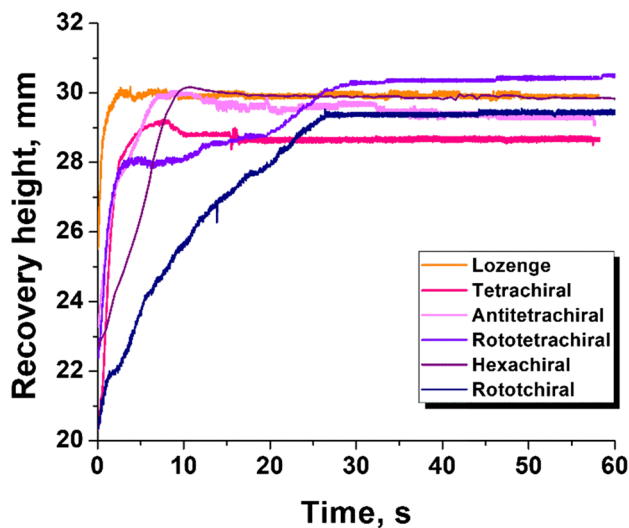


Fig. 6 Back-of-shape trials at 15 mm

the one capable of recovering the initial height more consistently. In terms of measurement variability, a greater dispersion is found for the rotochiral and hexachiral structures. Even the more contained elastic recovery can be associated with the rotochiral structure, perhaps due to the greater damage that is found in it as the number of compression cycles increases. The elastic recovery can be analyzed as a function of the density of the structure. In chiral geometries with lower density (lozenge), the springback is more marked than in structures with higher density (hexachiral and rotochiral). The lozenge structure recovers on average 20% more than the rotochiral, a structure which, from this point of view, is characterized by a less performing geometry.

3.1.3 Return of shape

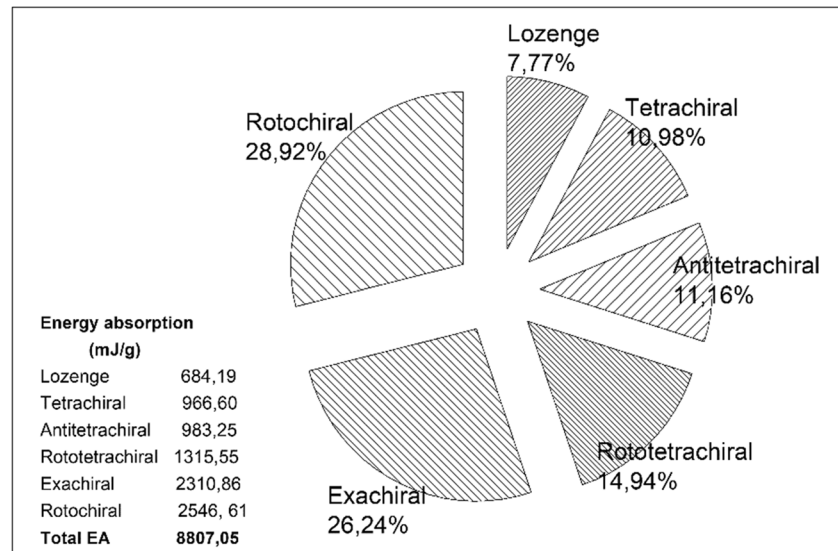
Figure 6 shows the shape recovery trend, analyzed after the springback. The lozenge structure recovers its initial shape more quickly presumably due to the limited damage suffered following repeated compression cycles. On the contrary, the Rotochiral structure takes more time to recover the initial height, this evidently because the damage caused by increasing the number of compression cycles, in terms of lesions or fractures, does not allow a practically instantaneous recovery as in the previous case. The observed trend of the shape recovery speed is however in line with the amount of deformation elastically recovered. Where the latter is greater, there is also a faster recovery of form. In terms of the maximum value of the height reached in the recovery phase, the rototetrachiral structure seems to be the most performing; however the greater value reached is linked to a higher value of the already starting height, i.e., downstream of the manufacturing process. The rotochiral structure, on the other hand, seems to be the one which, in addition to recovering less quickly, recovers its shape less effectively.

3.1.4 Absorption energy

After the compression tests and the measurements of the elastic recovery and the return of the shape, the value of the energy normalized with respect to the mass of the structure was calculated. To this end, the area under the force–displacement curves of the compression tests was considered. For this calculation, reference was made to the SEA (specific energy adsorption) parameter, which expresses the capacity of the structure to absorb energy per unit mass:

$$SEA = \frac{EA}{m}$$

where EA is the total energy absorbed by the chiral geometry, i.e., the area under the curve until the densification condition is reached [49], while m is the mass of the structure. Figure 7 shows the trend of the percentage of the total energy absorbed by the 6 structures in the compression tests at 15 mm deformation. The lozenge and tetrachiral structures have the least amount of energy absorbed, followed by the antitetrachiral and rototetrachiral structures. An almost double value can be observed for hexachiral and rotochiral structures. This is obviously due to the greater density of the latter which justifies a greater difficulty in going to impose deformations inside the structures. An energy that does not exceed the value of 1000 mJ/g corresponds to a relative density of 15 ÷ 16%, while for relative densities close to 20% the energy value is slightly more than double.

Fig. 7 Energy absorbed test at 15 mm

3.1.5 Analysis of the second loading cycle and shape recovery

Among the structures tested, three distinctive behaviors can be highlighted which are shown in Fig. 8 in terms of compression, elastic recovery, and shape recovery performed over two cycles. The structures designated to make the comparison were the lozenge, antitetrachiral, and rotochiral structures as they showed different trends. The lozenge structure records a very limited compressive force which, even for larger displacements, does not exceed 1000 N. This structure, however, allows the shape to be recovered to a greater extent and faster than the others. The rotochiral structure shows the strongest resistance force, around 3000 N. It can absorb a large part of the energy differently from the lozenge structure. However, the recovery appears to be reduced in terms of both elastic deformation and plastic deformation under thermal stimulation. Furthermore, a gap is observed in the values measured between the 1st and 2nd cycles which denotes such a level of damage to the structure that would prevent it to be used for a long time. Above all, in terms of stored specific energy and maximum recorded peak, it can be observed that the values corresponding to the 2nd cycle are in fact halved. An intermediate behavior can instead be observed for the antitetrachiral structure.

3.2 Analysis of the behavior of structures subjected to medium–low compressive stress.

3.2.1 Compression test 8 mm — eight cycles

The structures were also analyzed in terms of cyclic compression with medium–low load. Compression tests were

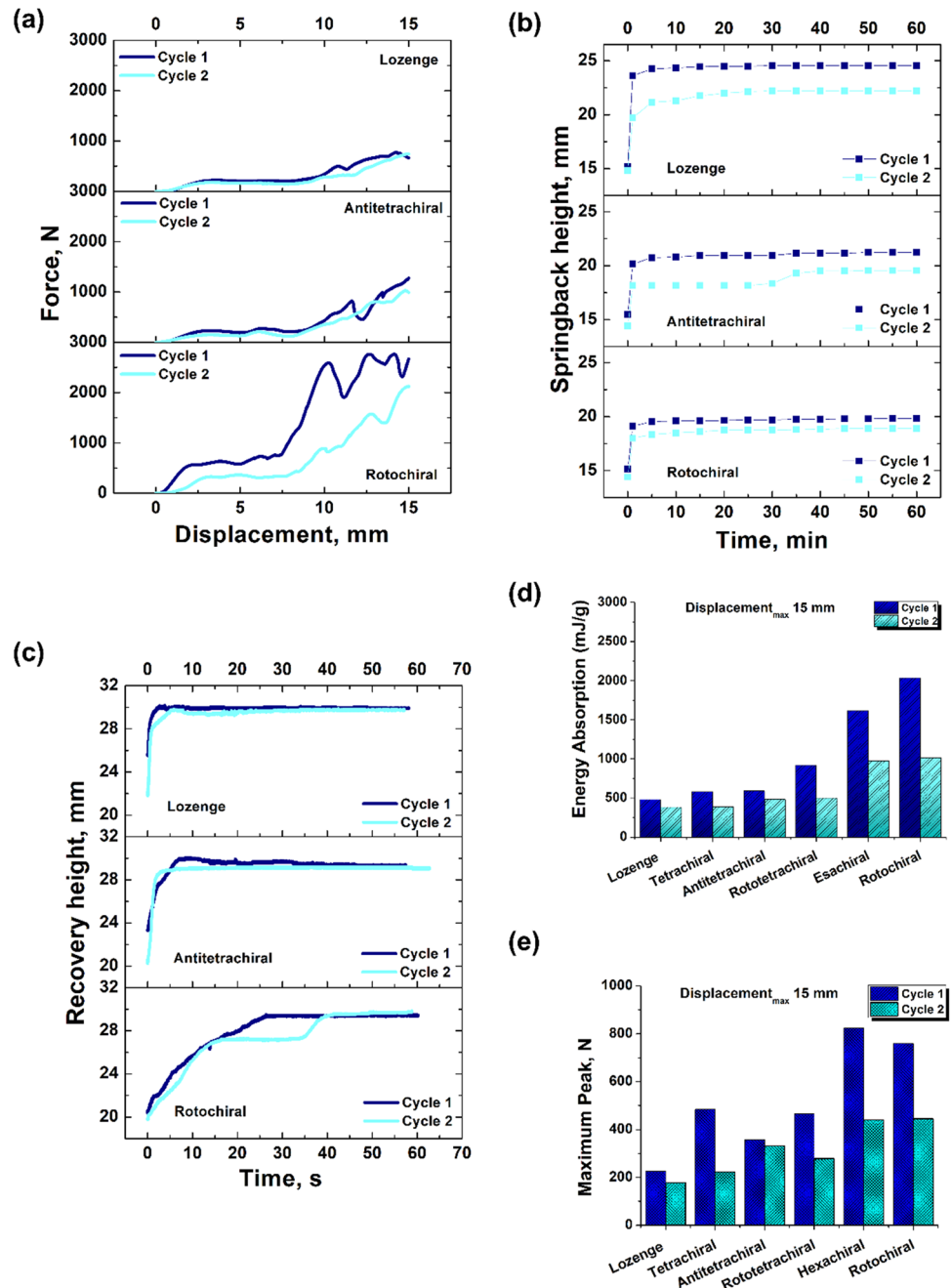
then carried out with the maximum displacement set at 8 mm. Following each compression cycle, recovery tests were carried out, both elastic (springback) at room temperature and shape, by means of thermal stimulation. Overall, as previously mentioned, 8 load cycles were analyzed.

Figure 9 shows the trends of the force–displacement curves, in particular for the previously designated structures, i.e., lozenge, antitetrachiral, and rotochiral, divided into three groups of analysis (I and II cycles–III, IV, and V cycles–VI, VII, and VIII cycles).

In the zoomed area provided at the top right for the three graphs, a decrease in load is observed between the first and second cycles. In the third cycle, the maximum load that the structure can bear is slightly higher. This aspect can be justified by the fact that the tests relating to the second and third cycles were carried out 48 h apart. A similar situation occurs between the fifth and sixth cycles. A justification of this experimental evidence can be related to a variation in the stiffness of the material due to a greater compaction of the structure following the application of an increasing number of load cycles. At the same time, it can be observed that the properties of polymeric materials such as PLA can be affected by recrystallization phenomena. PLA, like all polyesters, can recrystallize following the application of external stresses. The repeated load cycles to which the structures are subjected can therefore induce an increase in crystallinity by recrystallization of the material, resulting in an increase, sometimes high, in the stiffness and mechanical strength of the structures themselves. This aspect will be further explored with specific studies.

The rotochiral structure in the second compression cycle presents more defined peaks, suggesting that the presence of some damage on the structure caused by the previous cycles begins to influence its behavior. For the lozenge and

Fig. 8 Cycle 1° and 2° based on 15 mm of displacement: **a** Force–displacement curve; **b** springback height; **c** recovery height; **d** absorption energy; **e** maximum peak



antitetrachiral structure, the trend of the curves is more regular, with the maximum load decreasing as the compression cycles increase.

3.2.2 Springback test 8 mm — eight cycles

Figure 10 shows the value of the overall springback divided into the three analysis groups (I and II cycles–III, IV, and V cycles–VI, VII, and VIII cycles). The measurements were interrupted after 60 min, even if already after 40 min, the structures showed a complete elastic recovery. The graph

shows the average height values recovered elastically for each analysis group and referred to 22 mm, a height value theoretically related to the 8 mm deformation set during the compression test, although this cannot be guaranteed as the number of the load cycles increase.

The lozenge structure presents a high recovery in all three steps of the investigation, presumably due to the marked tendency towards packing of the polygonal geometry. Also, the antitetrachiral and hexachiral structures show an equally consistent springback, even if of a more marked level in the last two phases of the experiments.

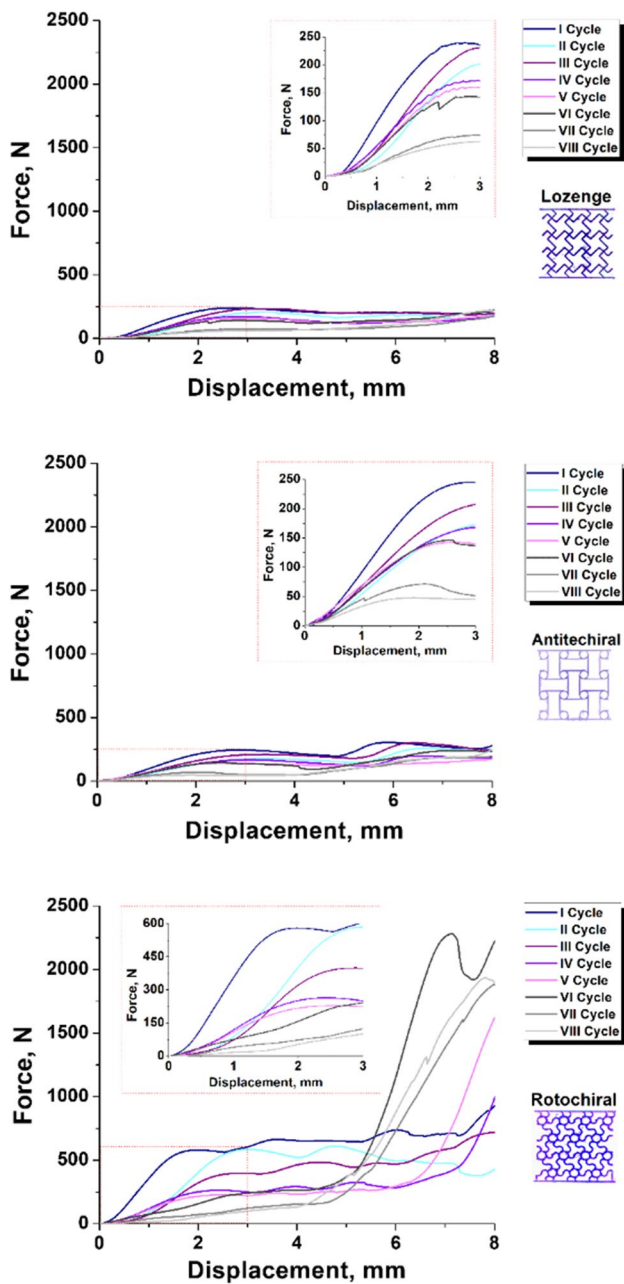
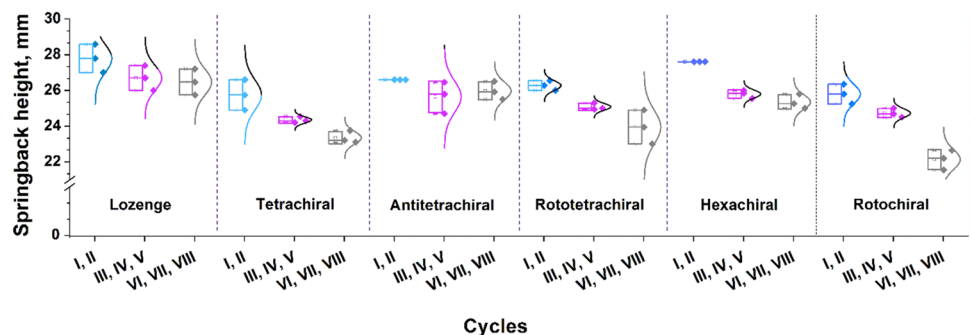


Fig. 9 Diagram force–displacement compression 8 mm: lozenge, antitetrachiral, and rotochiral

Fig. 10 Springback of each structure grouped by the three analysis groups for the 8 mm — eight cycle test



This could be attributed to the greater degree of damage achieved by the structures as the number of load cycles increases. Damage to the structure is caused by repeated compression cycles which, by damaging the connecting arms, leave a greater capacity for some elements of the cells to recover their shape in an unconstrained way.

3.2.3 Return of shape trial 8 mm — eight cycles

In the 8-mm shape return tests for all eight cycles, the height recovery process appears to evolve in an interval of about 60 s. In particular, the less dense structures such as antitet-rachiral and lozenge are plotted over a time of 55 s. The rotochiral structure is plotted over a 90-s interval, as shown in Fig. 11. From the curves in Fig. 11, the return of shape is limited for the structure that presents less damage following the repeated compression cycles. A maximum recovery of 3.5 mm was recorded for the lozenge structure for the fourth cycle, while lower values were recorded for the other structures. The trend of the curves for the lozenge structure shows a tendency to recover its shape quickly. After the first 15 s, in fact, a flat curve trend can be observed; i.e., no further increases in terms of height are made. In the case of the antitetrachiral and rotochiral structures, however, more discontinuous trends are highlighted due to the greater degree of damage that these structures undergo as the compression cycles increase. The considerations made previously in terms of springback continue to be valid also for the present cases.

3.2.4 Absorption energy

Figure 12 shows the comparison between the absorption energies measured respectively in the three experimental groups which include a total of the eight cycles analyzed for the compression tests with deformation of 8 mm. In general, between one cycle and the next, in five out of six structures, a load drop is observed, due to the loss of resistance and consequent reduction of the absorbed energy. Unlike the trend exhibited by these structures, in which a progressive decrease in the average value of absorption energy is

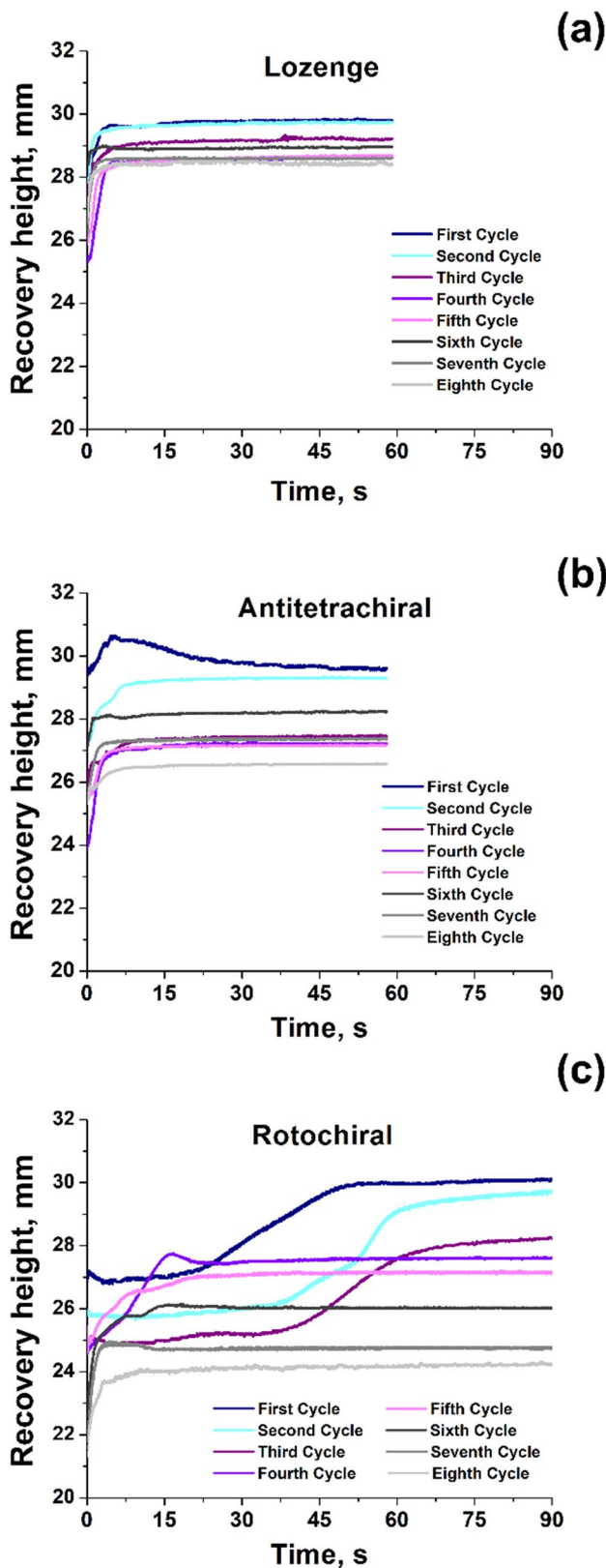


Fig. 11 Lozenge, antitetrachiral, and rotochiral shape return 8 mm test

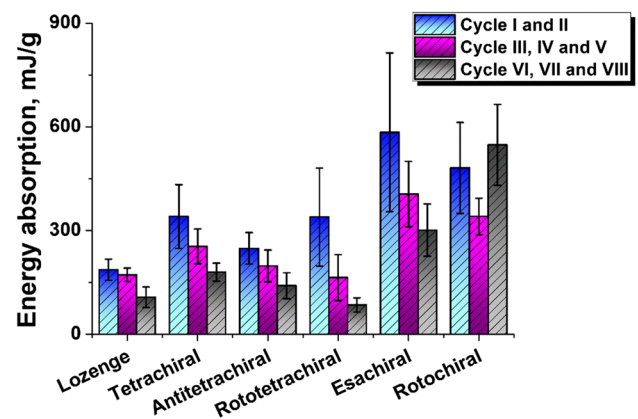


Fig. 12 Energy absorption test 8 mm — eight cycles

highlighted, the rotochiral structure shows an increase in the average value of absorption energy in the last three cycles (sixth, seventh, and eighth). This geometry, at the end of the last cycles, has little capacity to recover the initial shape due to the higher level of damage that the structure undergoes as the number of load cycles increases. This is evidenced by the previous trend shown in Fig. 11c. The final height of the specimen has taken on reduced values, and a consequent stacking of the cells in the structure can be seen. The significant increase in the measured force and therefore in the absorption energy is then to be attributed to the fact that, being the structure more compact in the last few cycles, it opposes more resistance to further compression. However, this greater resistance is to be attributed in an artificial way to the greater compactness of the structure and not to the design of the starting geometry of the same. The structure with the lowest energy variation is the lozenge, for which less damage is noted as the number of load cycles increases compared to the other structures.

4 Analysis of the higher density lozenge structure

From the analysis previously carried out, it can be highlighted that the lozenge structure exhibits a sufficiently stable and predictable response. Although the other chiral structures have superior mechanical properties and higher absorption energy than the latter, they are more sensitive to the problem of localized lesioning of the arms which makes them less reliable and reusable over several cycles. In Li et al. (2019) the lozenge structure was investigated for applications in cardiac stents. This study highlights a good symmetry of both integral and local structural deformation under the action of external loads. The structure itself is considered to be a good choice in the design and optimization of intravascular stents. By virtue of this

Fig. 13 Detail of the lozenge patterns: **a** 9 cells; **b** 16 cells

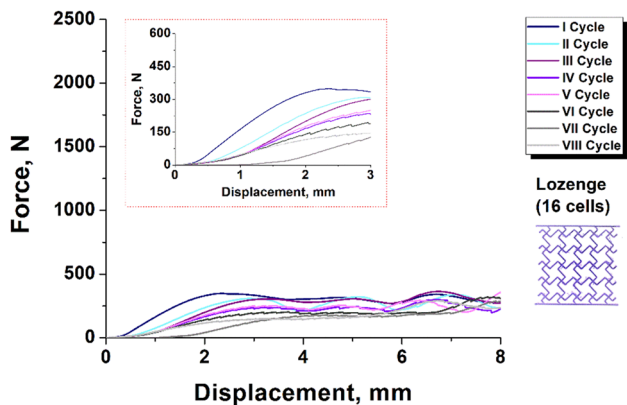
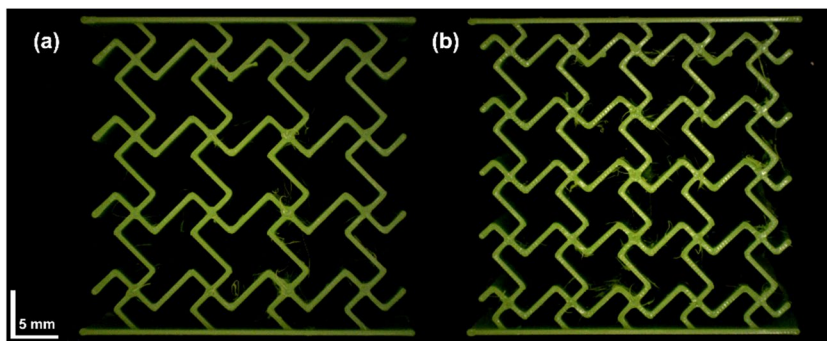


Fig. 14 Displacement curves for the lozenge compression tests dense grid tests at 8 mm — eight cycles

greater stability of the behavior of the lozenge structure to external stresses, the relative density of the structure was increased by 15%, bringing it to the value of 0.181, increasing the number of cells from 9 to 16, while maintaining the same symmetry and specimen size. In Fig. 13, an enlargement of the two patterns of the lozenge structure

is reported, less dense with 9 cells and more dense with 16 cells (Fig. 13a and b, respectively).

Figure 14 shows the trend of the force–displacement curves for the compression test of the denser lozenge structure. A trend like that already seen for the less dense structure can be noted, even though higher maximum load values are reached at each test. The structure after eight load cycles does not show a particular decay of the load value. The maximum peak value after 8 cycles stands at a value of no less than 20% of that corresponding to the first cycle, an indication that no fractures or significant lesions are induced in the structure. In the analysis of the springback (Fig. 15), the denser lozenge structure can elastically recover lower heights than the less dense structure. The reason is due to the ways in which this structure deforms during compression. In fact, the 16-cell lozenge structure tends to pack more during compression, compared to the less dense structure, resulting in greater difficulty in the elastic return phase. Finally, the trend of the return of shape is reported (Fig. 16), which, as seen for the springback, is characterized by lower values than the 9-cell lozenge structure, confirming the previous considerations.

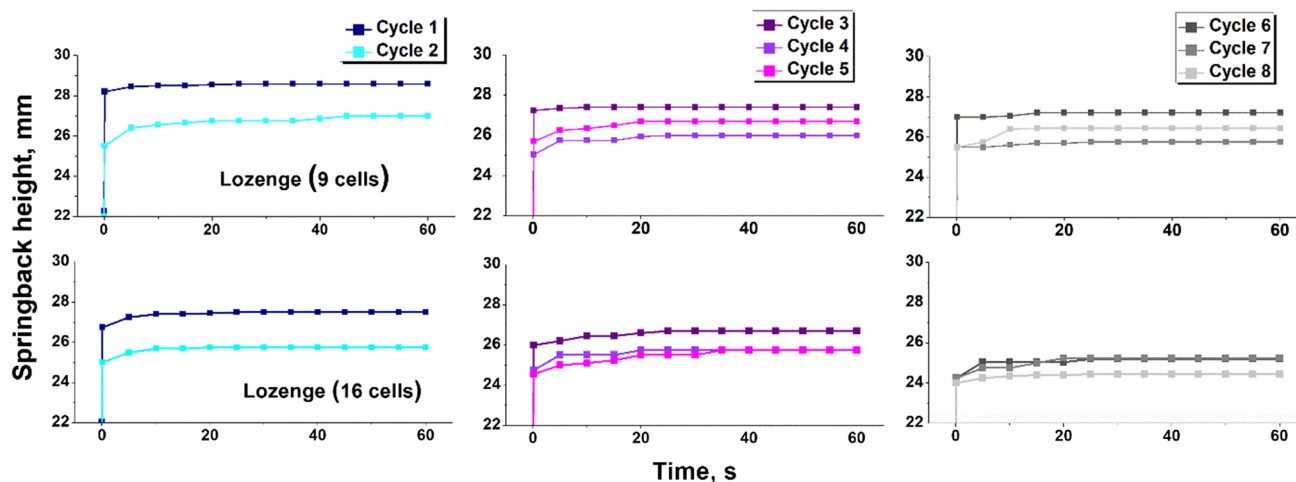


Fig. 15 Elastic recovery of dense lozenge and lozenge for the 3 days of experimentation 8 mm test — eight cycles

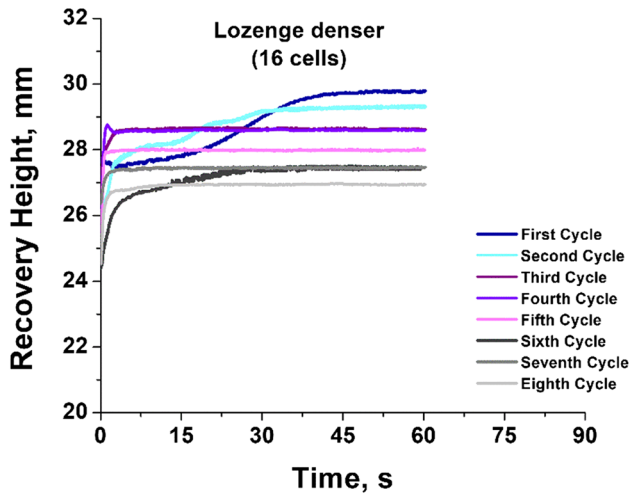


Fig. 16 Return of shape dense lozenge test at 8 mm — eight cycles

Therefore, for levels of damage to the structure that increase as the number of compression cycles increases, the structure itself achieves lower shape returns. The absorption energy for the denser structure is characterized by higher values, for all three experimental groups, as observable in Fig. 17a. In the last three cycles, i.e., from the sixth to the eighth cycle, the absorption energy values are comparable to those found in the first cycles of the lower density Lozenge structure. As previously seen for chiral structures, structures with higher density require higher absorption energies, as higher values of the maximum load are reached during the compression test.

For lozenge structure, unlike the non-polygonal chiral structures, however, there is no reduction in reliability because the progressively decreasing trend of energy as the cycles increase remains confirmed. This demonstrates how it can support higher loads, without exhibiting particular damage as the number of load cycles increases.

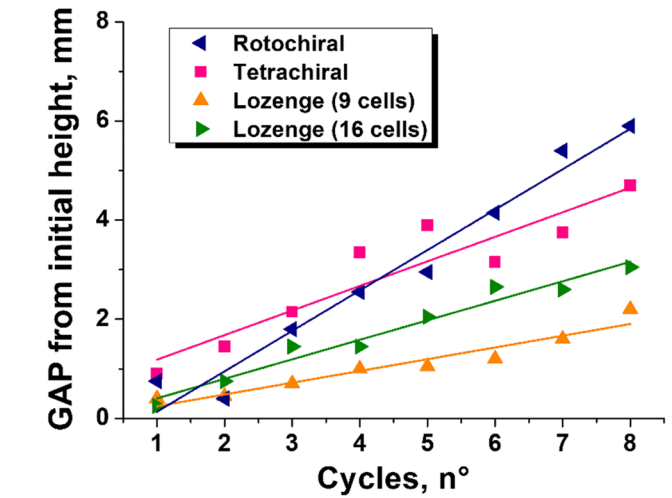
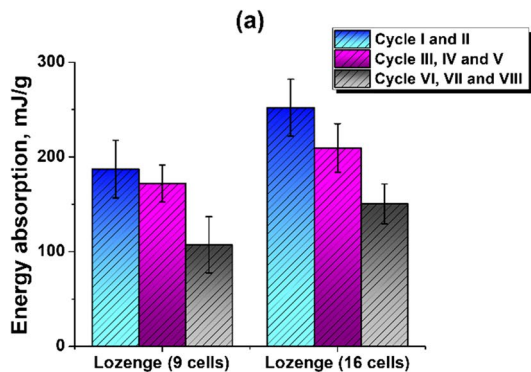


Fig. 18 Trend of the difference from the height value with respect to the initial test condition 8 mm — eight cycles

Finally, Fig. 17b shows the comparison between the maximum peak values for the three experimental groups, confirming that the higher density lozenge structure is capable of withstanding higher loads, which also justifies the higher energy absorption of the structure.

Figure 18 shows the trend of the height gap lost by the lozenge structures (9 cells), lozenge dense grid (16 cells), tetrachiral, and rotochiral structures with respect to the starting value and as the number of compression cycles varies. In correspondence with the first cycle, all the structures manage to recover a large part of the imprinted deformation going to almost completely restore their shape. The gap found on the heights of the different samples is, in this case, never greater than 1 mm. However, by reiterating the application of the compressive load over several cycles, a loss of recovery capacity is observed which has an increasing linear trend.

The tetrachiral structure, and even more so the rotochiral structure, has less ability to recover the shape because they

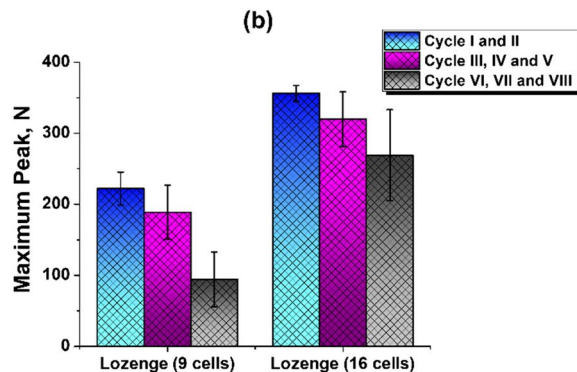


Fig. 17 a Comparison of energy absorbed between Lozenge structures tested at 8 mm — eight cycles. b Comparison of maximum peak lozenge and dense lozenge trials at 8 mm — eight cycles

appear to be the structures that present the most significant damages among the structures analyzed with increasing load cycles. The denser version of the lozenge structure presents an intermediate behavior, while the lower density lozenge structure has higher recovery capacities, as shown by the lower slope of the representative line of the gap of the heights of the samples in Fig. 18. This aspect can be attributed to the fact that the lower density lozenge geometry allows for greater flexibility in deformation. This determines during the repeated compression cycles less damage to the structure, which results in a more stable response. In fact, after eight compression cycles, it loses less than 2 mm compared to the starting value.

5 Conclusions

In the present study, six chiral structures were analyzed in terms of their mechanical deformation behavior under quasi-static compressive loading and subsequent shape recovery, repeated over several cycles. It was possible to define the maximum deformation, below which the damage induced on the structures by the repeated load cycles does not affect the reliability of the structure. Following the compression tests, the evaluation of elastic recovery (springback) and shape recovery was carried out. In the case of springback, there is a correlation between damage and recovered height: the more the structure is damaged after repeated compression cycles, the lower its ability to exhibit a high springback will be. Similarly, as far as the recovery of shape is concerned, the level of damage induced in the structure by the repeated load cycles considerably affects the recovery of the initial height. The chiral geometries characterized by the presence of circles in the structure have shown better mechanical properties, with the same mass and density than the chiral polygonal structure, as well as higher absorption energy. As the number of load cycles increases, this benefit tends to decrease, due to the increasing damage encountered on non-polygonal chiral structures. The lozenge structure does not boast excellent mechanical behavior, but it is the most reliable as the number of load cycles increases, exhibiting less deformation and damage. On the one hand, the lozenge structure has a lower capacity to absorb energy, but the limited damage it suffers as load cycles increase, allow it to obtain a reduced difference in energy absorbed between two subsequent cycles. The denser 16-cell Lozenge structure confirms the previous considerations. In fact, a 15% increase in density leads to a worsening of the damage caused to the structure as the number of load cycles increases. However, these damages do not lead to specimen failure. Furthermore, the absorption energy increases with respect to the structure with the lowest density.

In conclusion, it is possible to state that non-polygonal chiral structures perform better for a low number of load cycles. However, under repeated strain, they collapse and become permanently deformed. Polygonal chiral structures, on the other hand, perform better as the number of cycles increases, as they are more resistant to cyclic stresses, without being substantially damaged up to a greater number of load cycles.

Future investigations will focus on the best 1 or 2 structures to focus the experimental plan on the effect of the wall thickness and layers orientation. In addition, further experiments will be devoted to understand the role of the boundary effects of each structure by increasing the number of cells from 4 and 9 (herein investigated) to 16 and, possibly, more. This should allow to further clarify the role of the boundary effects on the homogeneity of the deformation of each specific structure when submitted to repeated compressive loads.

Author contribution All authors contributed to the study conception and design. Material preparation, data collection, and analysis were performed by Gisario Annamaria and Desole Maria Pia. The first draft of the manuscript was written by Gisario Annamaria and Desole Maria Pia, and all authors commented on previous versions of the manuscript. The manuscript was revised by Gisario Annamaria and Massimiliano Barletta. All authors read and approved the final manuscript.

Funding Open access funding provided by Università degli Studi Roma Tre within the CRUI-CARE Agreement.

Declarations

Conflict of interest The authors declare no competing interests.

Open Access This article is licensed under a Creative Commons Attribution 4.0 International License, which permits use, sharing, adaptation, distribution and reproduction in any medium or format, as long as you give appropriate credit to the original author(s) and the source, provide a link to the Creative Commons licence, and indicate if changes were made. The images or other third party material in this article are included in the article's Creative Commons licence, unless indicated otherwise in a credit line to the material. If material is not included in the article's Creative Commons licence and your intended use is not permitted by statutory regulation or exceeds the permitted use, you will need to obtain permission directly from the copyright holder. To view a copy of this licence, visit <http://creativecommons.org/licenses/by/4.0/>.

References

1. Chen J, Hu S, Zhu S, Li T (2022) Metamaterials: from fundamental physics to intelligent design. *Interdisc Mater*. <https://doi.org/10.1002/idm2.12049>
2. Frenzel T, Kadic M, Wegener M (2017) Three-dimensional mechanical metamaterials with a twist. *Science* 358:1072–1074. <https://doi.org/10.1126/science.aao4640>
3. Jia Z, Liu F, Jiang X, Wang L (2020) Engineering lattice metamaterials for extreme property, programmability, and multifunctionality. *J Appl Phys* 127:150901. <https://doi.org/10.1063/5.0004724>

4. Liu Y, Zhang X (2011) Metamaterials: a new frontier of science and technology. *Chem Soc Rev* 40:2494–2507. <https://doi.org/10.1039/C0CS00184H>
5. Iwanaga M (2012) Photonic metamaterials: a new class of materials for manipulating light waves. *Sci Technol Adv Mater* 13:053002. <https://doi.org/10.1088/1468-6996/13/5/053002>
6. Tawalbeh M, Khan HA, Hajar AA, Al-Othman A (2022) Applications of metamaterials, in: Olabi, A.-G. (Ed.), *Encyclopedia of smart materials*. Elsevier, Oxford, pp. 11–24. <https://doi.org/10.1016/B978-0-12-815732-9.00089-9>
7. Valipour A, Kargozarfard MH, Rakhshi M, Yaghootian A, Sedighi HM (2022) Metamaterials and their applications: an overview. *Proceed Inst Mech Eng, Part L: J Mater: Design Appl* 236:2171–2210. <https://doi.org/10.1177/1464420721995858>
8. Askari M, Hutchins DA, Thomas PJ, Astolfi L, Watson RL, Abdi M, Ricci M, Laureti S, Nie L, Freear S, Wildman R, Tuck C, Clarke M, Woods E, Clare AT (2020) Additive manufacturing of metamaterials: a review. *Additive Manuf* 36:101562. <https://doi.org/10.1016/j.addma.2020.101562>
9. Cao D, Malakooti S, Kulkarni VN, Ren Y, Liu Y, Nie X, Qian D, Griffith DT, Lu H (2022) The effect of resin uptake on the flexural properties of compression molded sandwich composites. *Wind Energy* 25:71–93. <https://doi.org/10.1002/we.2661>
10. Cao D, Malakooti S, Kulkarni VN, Ren Y, Lu H (2021) Nanoindentation measurement of core–skin interphase viscoelastic properties in a sandwich glass composite. *Mech Time-Depend Mater* 25:353–363. <https://doi.org/10.1007/s11043-020-09448-y>
11. Lu C, Hsieh M, Huang Z, Zhang C, Lin Y, Shen Q, Chen F, Zhang L (2022) Architectural design and additive manufacturing of mechanical metamaterials: a review. *Engineering*. <https://doi.org/10.1016/j.eng.2021.12.023>
12. Wang X, Xu T, de Andrade MJ, Rampalli I, Cao D, Haque M, Roy S, Baughman RH, Lu H (2021) The interfacial shear strength of carbon nanotube sheet modified carbon fiber composites, in: Silberstein, M., Amirkhizi, A. (Eds.), *Challenges in mechanics of time dependent materials, Volume 2, Conference Proceedings of the Society for Experimental Mechanics Series*. Springer International Publishing, Cham, pp. 25–32. https://doi.org/10.1007/978-3-030-59542-5_4
13. Dhinakaran V, Manoj Kumar KP, Bupathi Ram PM, Ravichandran M, Vinayagamoorthy M (2020) A review on recent advances in fused deposition modeling. *Mater Today: Proceed, First Int conference Adv Lightweight Mater Struct* 27:752–756. <https://doi.org/10.1016/j.matpr.2019.12.036>
14. Li S, Hassanin H, Attallah MM, Adkins NJE, Essa K (2016) The development of TiNi - based negative Poisson's ratio structure using selective laser melting. *Acta Mater* 105:75–83. <https://doi.org/10.1016/j.actamat.2015.12.017>
15. Wadley HNG, Fleck NA, Evans AG (2003) Fabrication and structural performance of periodic cellular metal sandwich structures. *Composites Sci Technol, Porous Mater* 63:2331–2343. [https://doi.org/10.1016/S0266-3538\(03\)00266-5](https://doi.org/10.1016/S0266-3538(03)00266-5)
16. Surjadi JU, Gao L, Du H, Li X, Xiong X, Fang NX, Lu Y (2019) Mechanical metamaterials and their engineering applications. *Adv Eng Mater* 21:1800864. <https://doi.org/10.1002/adem.201800864>
17. Leary M, Mazur M, Elambasseril J, McMillan M, Chirent T, Sun Y, Qian M, Easton M, Brandt M (2016) Selective laser melting (SLM) of AlSi12Mg lattice structures. *Mater Des* 98:344–357. <https://doi.org/10.1016/j.matdes.2016.02.127>
18. Maskery I, Aboulkhair NT, Aremu AO, Tuck CJ, Ashcroft IA, Wildman RD, Hague RJM (2016) A mechanical property evaluation of graded density Al-Si10-Mg lattice structures manufactured by selective laser melting. *Mater Sci Eng, A* 670:264–274. <https://doi.org/10.1016/j.msea.2016.06.013>
19. Yan C, Hao L, Hussein A, Young P, Huang J, Zhu W (2015) Microstructure and mechanical properties of aluminum alloy cellular lattice structures manufactured by direct metal laser sintering. *Mater Sci Eng, A* 628:238–246. <https://doi.org/10.1016/j.msea.2015.01.063>
20. Zhang J, Lu G, You Z (2020) Large deformation and energy absorption of additively manufactured auxetic materials and structures: a review. *Composites Part B: Eng* 201:108340. <https://doi.org/10.1016/j.compositesb.2020.108340>
21. Han Z, Wang Z, Wei K, 2022. Shape morphing structures inspired by multi-material topology optimized bi-functional metamaterials. *Composite Struct* 300. <https://doi.org/10.1016/j.compstruct.2022.116135>
22. Kelkar PU, Kim HS, Cho K-H, Kwak JY, Kang C-Y, Song H-C (2020) Cellular auxetic structures for mechanical metamaterials: a review. *Sensors* 20:3132. <https://doi.org/10.3390/s20113132>
23. Lu C, Qi M, Islam S, Chen P, Gao S, Xu Y, Yang X (2018) Mechanical performance of 3D-printing plastic honeycomb sandwich structure. *Int J of Precis Eng and Manuf-Green Tech* 5:47–54. <https://doi.org/10.1007/s40684-018-0005-x>
24. Mousanezhad D, Haghpanah B, Ghosh R, Hamouda AM, Nayeb-Hashemi H, Vaziri A (2016) Elastic properties of chiral, anti-chiral, and hierarchical honeycombs: a simple energy-based approach. *Theor Appl Mech Lett* 6:81–96. <https://doi.org/10.1016/j.taml.2016.02.004>
25. Papadopolou A, Laucks J, Tibbits S (2017) Auxetic materials in design and architecture. *Nat Rev Mater* 2. <https://doi.org/10.1038/natrevmats.2017.78>
26. Sorrentino A, Castagnetti D, Mizzi L, Spaggiari A (2022) Bio-inspired auxetic mechanical metamaterials evolved from rotating squares unit. *Mechanics Mater* 173:104421. <https://doi.org/10.1016/j.mechmat.2022.104421>
27. Wang A-J, McDowell DL (2004) In-plane stiffness and yield strength of periodic metal honeycombs. *J Eng Mater Technol* 126:137–156. <https://doi.org/10.1115/1.1646165>
28. Wu W, Hu W, Qian G, Liao H, Xu X, Berto F (2019) Mechanical design and multifunctional applications of chiral mechanical metamaterials: a review. *Mater Design* 180:107950. <https://doi.org/10.1016/j.matdes.2019.107950>
29. Zarek M, Layani M, Cooperstein I, Sachyani E, Cohn D, Magdassi S (2016) 3D printing of shape memory polymers for flexible electronic devices. *Adv Mater* 28:4449–4454. <https://doi.org/10.1002/adma.201503132>
30. Zhang C, Cai D, Liao P, Su J-W, Deng H, Vardhanabuthi B, Ulery BD, Chen S-Y, Lin J (2021) 4D Printing of shape-memory polymeric scaffolds for adaptive biomedical implantation. *Acta Biomater* 122:101–110. <https://doi.org/10.1016/j.actbio.2020.12.042>
31. Lubombo C, Huneault MA (2018) Effect of infill patterns on the mechanical performance of lightweight 3D-printed cellular PLA parts. *Mater Today Commun* 17:214–228. <https://doi.org/10.1016/j.mtcomm.2018.09.017>
32. McGregor DJ, Tawfik S, King WP (2019) Mechanical properties of hexagonal lattice structures fabricated using continuous liquid interface production additive manufacturing. *Addit Manuf* 25:10–18. <https://doi.org/10.1016/j.addma.2018.11.002>
33. Santos FA, Rebelo H, Coutinho M, Sutherland LS, Cismasiu C, Farina I, Fraternali F (2021) Low velocity impact response of 3D printed structures formed by cellular metamaterials and stiffening plates: PLA vs. PETg. *Composite Struct* 256:113128. <https://doi.org/10.1016/j.compstruct.2020.113128>
34. González-Hernández CM, Sarabia-Vallejos MA, Rodríguez-Hernández J (2019) Polymers for additive manufacturing and 4D-printing: materials, methodologies, and biomedical applications. *Prog Polym Sci* 94:57–116. <https://doi.org/10.1016/j.progpolymsci.2019.03.001>

35. Rezvani Ghomi E, Khosravi F, Saedi Ardahaei A, Dai Y, Neisiany RE, Foroughi F, Wu M, Das O, Ramakrishna S (2021) The life cycle assessment for polylactic acid (PLA) to make it a low carbon material. *Polymers (Basel)* 13:1854. <https://doi.org/10.3390/polym13111854>
36. Herzog D, Seyda V, Wycisk E, Emmelmann C (2016) Additive manufacturing of metals. *Acta Mater* 117:371–392. <https://doi.org/10.1016/j.actamat.2016.07.019>
37. Barletta M, Gisario A, Mehrpouya M (2021) 4D printing of shape memory polylactic acid (PLA) components: investigating the role of the operational parameters in fused deposition modeling (FDM). *J Manuf Process* 61:473–480. <https://doi.org/10.1016/j.jmapro.2020.11.036>
38. Mehrpouya M, Edelijan T, Ibrahim M, Mohebsahedin A, Gisario A, Barletta M (2022) Functional behavior and energy absorption characteristics of additively manufactured smart sandwich structures. *Adv Eng Mater* 24:2200677. <https://doi.org/10.1002/adem.202200677>
39. Yousefi A, Jolaiy S, Lalegani Dezaki M, Zolfagharian A, Serjouei A, Bodaghi M (2022) 3D-printed soft and hard meta-structures with supreme energy absorption and dissipation capacities in cyclic loading conditions. *Adv Eng Mater* 2201189. <https://doi.org/10.1002/adem.202201189>
40. Hou S, Li T, Jia Z, Wang L (2018) Mechanical properties of sandwich composites with 3d-printed auxetic and non-auxetic lattice cores under low velocity impact. *Mater Des* 160:1305–1321. <https://doi.org/10.1016/j.matdes.2018.11.002>
41. Li C, Lei H, Zhang Z, Zhang X, Zhou H, Wang P, Fang D (2020) Architecture design of periodic truss-lattice cells for additive manufacturing. *Additive Manuf* 34:101172. <https://doi.org/10.1016/j.addma.2020.101172>
42. Valerga AP, Batista M, Salguero J, Girot F (2018) Influence of PLA filament conditions on characteristics of FDM parts. *Materials* 11:1322. <https://doi.org/10.3390/ma11081322>
43. Hanon MM, Zsidai L (2021) Comprehending the role of process parameters and filament color on the structure and tribological performance of 3D printed PLA. *J Market Res* 15:647–660. <https://doi.org/10.1016/j.jmrt.2021.08.061>
44. Hanon MM, Zsidai L, Ma Q (2021) Accuracy investigation of 3D printed PLA with various process parameters and different colors. *Mater Today: Proceed, 3rd Int Conference Mater Eng Sci* 42:3089–3096. <https://doi.org/10.1016/j.matpr.2020.12.1246>
45. Masood SH, Song WQ (2004) Development of new metal/polymer materials for rapid tooling using fused deposition modelling. *Mater Des* 25:587–594. <https://doi.org/10.1016/j.matdes.2004.02.009>
46. Najafi M, Ahmadi H, Liaghat G (2021) Experimental investigation on energy absorption of auxetic structures. *Mater Today: Proceed, 12th Int Conference Composite Sci Technol* 34:350–355. <https://doi.org/10.1016/j.matpr.2020.06.075>
47. Orhan SN, Erden S (2022) Numerical investigation of the mechanical properties of 2D and 3D auxetic structures. *Smart Master. struct.* 31:065011. <https://doi.org/10.1088/1361-665X/ac6918>
48. Tancogne-Dejean T, Spierings AB, Mohr D (2016) Additively-manufactured metallic micro-lattice materials for high specific energy absorption under static and dynamic loading. *Acta Mater* 116:14–28. <https://doi.org/10.1016/j.actamat.2016.05.054>
49. Mohsenizadeh M, Gasbarri F, Munther M, Beheshti A, Davami K (2018) Additively manufactured lightweight metamaterials for energy absorption. *Mater Des* 139:521–530. <https://doi.org/10.1016/j.matdes.2017.11.037>

Publisher's note Springer Nature remains neutral with regard to jurisdictional claims in published maps and institutional affiliations.